Fourier-Based Preconditioning for 3D Two-Fluid Computations and Scaling

C. R. Sovinec

University of Wisconsin-Madison

pre-APS CEMM Meeting

Dallas, Texas November 16, 2008

Outline

- Introduction
- Preconditioning strategies
- Parallel scaling
- Internal kink application
- Conclusions

Introduction: NIMROD's 'implicit leapfrog' algorithm is tailored for coefficients of high-order spatial expansions.

- A plane (poloidal) of 2D spectral elements and finite Fourier series in the periodic coordinate (toroidal angle) allow spectral convergence.
- Implicit advances require solution of large algebraic systems at each step.
    - With symmetric geometry and equilibria, linear computations solve a separate linear system for each Fourier component, like separate 2D computations.
    - Matrices for nonlinear 3D computations have matrix elements that couple different Fourier components. They are <u>smaller</u> than the matrix elements for the poloidal-plane coupling <u>by at least one factor of the perturbation amplitude</u>.
    - Our use of FFTs to compute Fourier-component couplings scales well in production calculations, but algebraic representation of the complete '3D' matrix is not practical.
- Krylov-space solvers iterate with matrix-vector product operations but not elements of the matrix. Approximate matrices are used to 'precondition.'

Hall-MHD in 3D has been problematic because fluctuations do not contribute to the diagonal of the **B**-advance operator, and the whistler is the fastest mode of the system.

• With **A** being a test function and dropping surface terms,

$$-\frac{\Delta t}{2}\int \mathbf{A}\cdot\nabla\times\left(\frac{1}{\mu_0 \bar{n} e}\tilde{\mathbf{B}}^{j+1/2}\times\nabla\times\Delta\mathbf{B}\right)dVol =$$

$$-\frac{\Delta t}{2}\int \frac{1}{\mu_0 \bar{n} e}\left(\nabla\times\mathbf{A}\right)\cdot\tilde{\mathbf{B}}^{j+1/2}\times\left(\nabla\times\Delta\mathbf{B}\right)dVol$$

• When the test and trial functions are expanded, the resulting matrix has mixed partials on the diagonal due to the cross product.

• With a Fourier expansion, the first-order toroidal derivatives lead to imaginary terms on the diagonal.

  • The operator is non-Hermitian.
  • It detracts from diagonal dominance when $\tilde{\mathbf{B}}^{j+1/2}$ and Δt are sufficiently large.

Aside: implicit electron inertia, even at physical m_e/m_i ratios, helps matrix condition numbers.

• The HPD part of our system is increased by adding the $\frac{1}{\varepsilon_0 \omega_e^2}\frac{\partial}{\partial t}\mathbf{J}$ part of electron inertia.

$$\Delta\mathbf{B} - \frac{\Delta t}{2}\nabla\times\left(\mathbf{V}^{j+1}\times\Delta\mathbf{B}\right) + \frac{\Delta t}{2}\nabla\times\frac{1}{\bar{n}e}\left(\mathbf{J}^{j+1/2}\times\Delta\mathbf{B} + \Delta\mathbf{J}\times\mathbf{B}^{j+1/2}\right)$$

$$+\Delta t\,\nabla\times\left(\frac{\eta}{2} + \underline{\frac{d_e^2}{\Delta t}}\right)\nabla\times\Delta\mathbf{B} - \Delta t\,\kappa_{divb}\nabla\nabla\cdot\Delta\mathbf{B}$$

for the lhs of the **B**-advance, also showing the divergence cleaning term. The electron skin depth is $d_e = c/\omega_e$.

• Physically, electron inertia leads to the electron cyclotron resonance, which keeps the *R*-mode phase speed from growing indefinitely as k_{max} increases with spatial resolution.

• This helps limit stiffness, hence condition numbers, in two-fluid computations.

Preconditioning Strategies

NIMROD's standard strategy is to use only the large matrix elements that couple coefficients of the same Fourier index.

• This approach works well for semi-implicit MHD with predictor/corrector advection where matrices are HPD [JCP **195**, 355 (2004)] and for semi-implicit MHD with implicit advection and/or gyroviscosity, where the non-Hermitian part is small.

Three new (for NIMROD) strategies for substantially non-HPD matrices have been tested this past year. Two have been discarded:

1. Polynomial approximation can reduce GMRES iteration in the two-fluid **B**-advance, but its iteration is just as costly.
2. Evaluating 2D poloidal 'slices' at a set of uniformly spaced toroidal angles was intended to complement the standard Fourier-based scheme.

    • Stand-alone 'slicing' is effective for sufficiently small Δt.

    • At Δt of interest for production simulations, lack of diagonal dominance on the toroidal grid prevents convergence, even when used as a multiplicative step with the standard Fourier-based scheme.

3) An approach based on limited off-diagonal Fourier coupling has advantages over the other two strategies.

- For block Gauss-Seidel preconditioning, the Fourier representation helps keep the spectral radius of $(D+L)^{-1}U$ less than 1 at large time-step, unlike the slicing strategy. [Here, the notation refers to block-based splitting $A=L+D+U$.]
- With limited couplings, matrix elements can be generated, and matrix-vector products are fast relative to full matrix-free product operations.
    - The required coding for these matrices is a generalization of existing code for the diagonal-in-Fourier systems.
    - When used in iteration, these matrices are not factored.
- Generating matrix elements is computationally intensive but scales well in parallel. [Generation of full convolution matrices is not practical, however, even in parallel.]
- The extra communication during Jacobi/Gauss-Seidel iteration (preconditioner looping) is point-to-point.

The limited Fourier coupling helps avoid increasing GMRES iteration as toroidal resolution is increased.

• The test case here is a small two-fluid 1/1 cylindrical kink. [The physics is helically symmetric, but NIMROD treats it as a 3D computation.]

• Here, the representation is 9×9 biquintic, and $\Delta t/\tau_{Hp} = 2$.

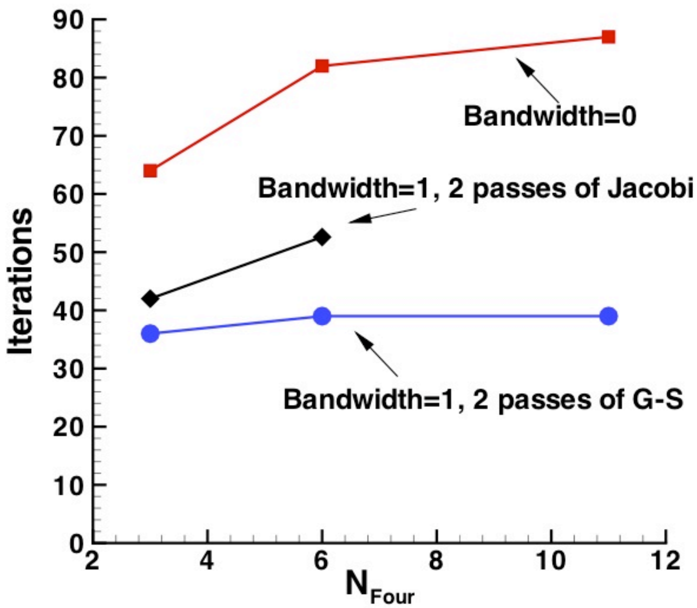

G-S passes makes the iteration nearly independent of the number of Fourier comps (N_{Four}) in this case.

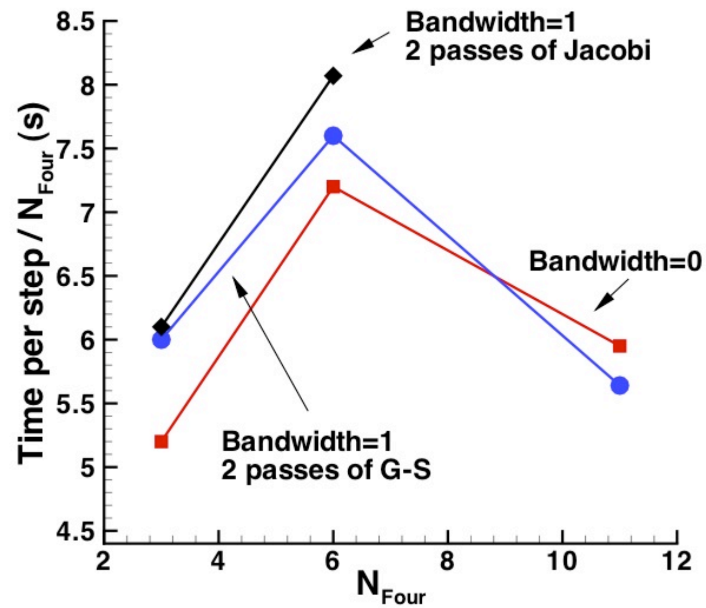

Serial CPU time is shown per Fourier comp. Data at N_{Four}=11 is from Bassi unlike others.

• The near-constant iteration count with increasing N_{Four} is important.

• This case is dominated by n=1; others may be more challenging.

Parallel Scaling

Improving resolution requires increasing use of parallelism that is available in new multi-core massively parallel computers.

• The new preconditioner has been developed to provide good scaling with NIMROD's two types of domain decomposition (poloidal blocks and Fourier layers).

• Application is a two-fluid kink in the early nonlinear stage; $\Delta t = 0.1\ \tau_A$.

• Results are from the Cray XT4 at NERSC ("Franklin"), quad-core.

• Parameters provide a weak scaling of a production computation.

• New preconditioner help keep GMRES iterations fixed with increasing N_{Four}.

• Largest computation has 1.8×10^8 degrees of freedom (coefficients of the high-order representation) and exceeds the 1-TFlop level of actual performance.

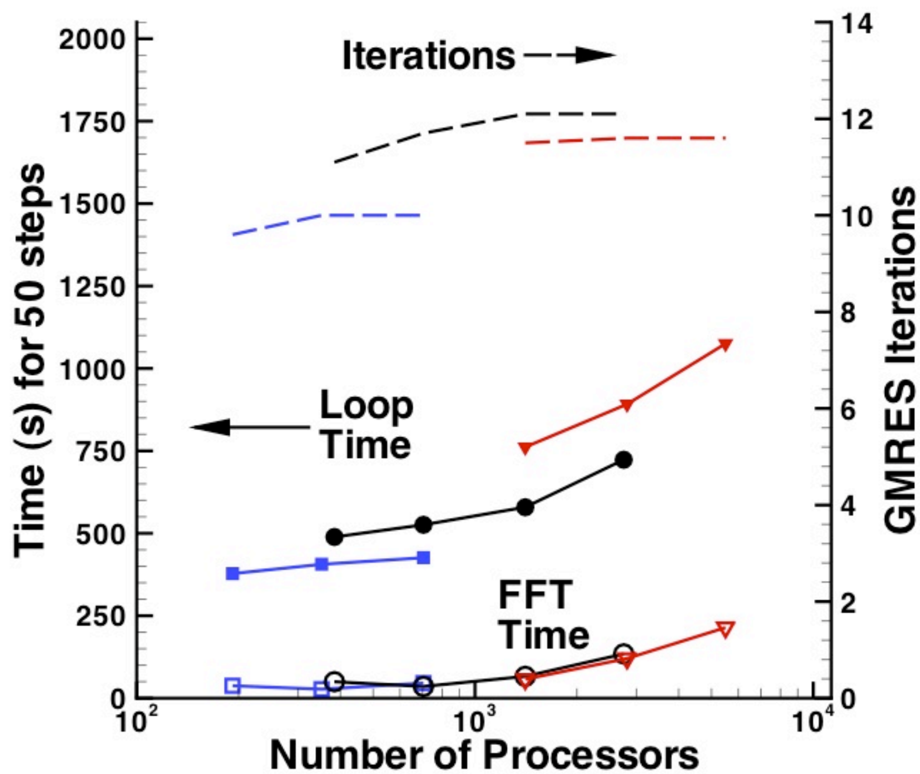

Blue: 32 blocks; Black: 64 blocks; Red: 128 blocks. Within color shows increasing N_{Four}.

Memory may be the limiting factor in this scaling.

• Results include recent efficiency improvements that reduce latency in the communication operations before and after FFTs.

• The two types of decomposition are algorithmically independent.

• Both 64- and 128-block sets are scaled to 86 Fourier components with 2 components per layer.

• Computations with 128 blocks approach maximum average available memory per core.

• Improvements in new release of SuperLU_DIST may help.

• LBL group (X. Li) is developing an ILU version of SuperLU_DIST, which may be more efficient for preconditioning.

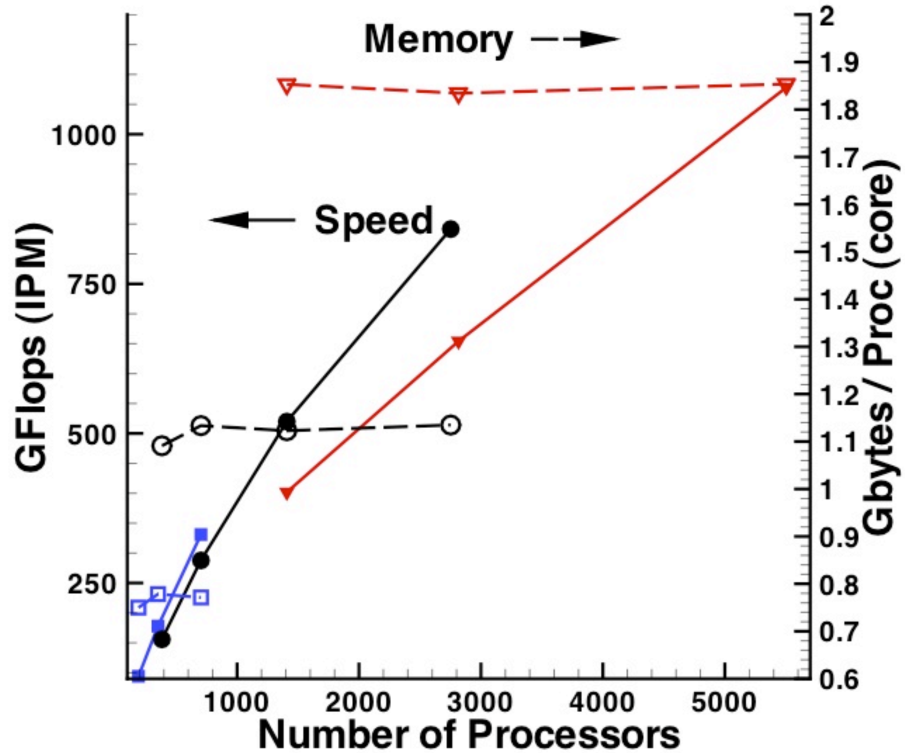

Computational performance and memory use in scaling study.

Internal Kink Application

Application of NIMROD to the nonlinear two-fluid internal-kink is both a nonlinear benchmark and a research study.

- Cylindrical results (see poster BP6.00042) can be benchmarked against others.
    - Germaschewski will present the same type of fast reconnection behavior from a full model in presentation GI1.00004.
- Toroidal results summarized here may be new.

Simulations of the internal kink in toroidal geometry investigate inherently three-dimensional evolution.

- Equilibria are generated with the new NIMEQ code: E. Howell, BP6.00041.
- Profiles for the circular cross-section, R/a=4 torus are specified as P=const (β=5×10^{-3}) and

  $$F = 3.44 + 0.12(1-\psi) + 0.064\psi(\psi-1)$$

  where ψ is the normalized ring flux.
- Here $q(0)$=0.97, $q(a)$=1.61.
- Other parameters are:

$$S = \tau_r / \tau_{Hp} = 1.48 \times 10^6 \quad \tau_{Hp} \equiv 2\pi a^2 \sqrt{\mu_0 \rho} / \mu_0 I_p$$

$$d_e = 5 \times 10^{-3} \quad \delta = d_i/2 = 0.11 \quad \rho_s = 1.5 \times 10^{-2}$$

$$\mu_0 \nu_{iso} / \eta = \mathrm{Pm} = 0.1 \quad T_i \cong 0$$

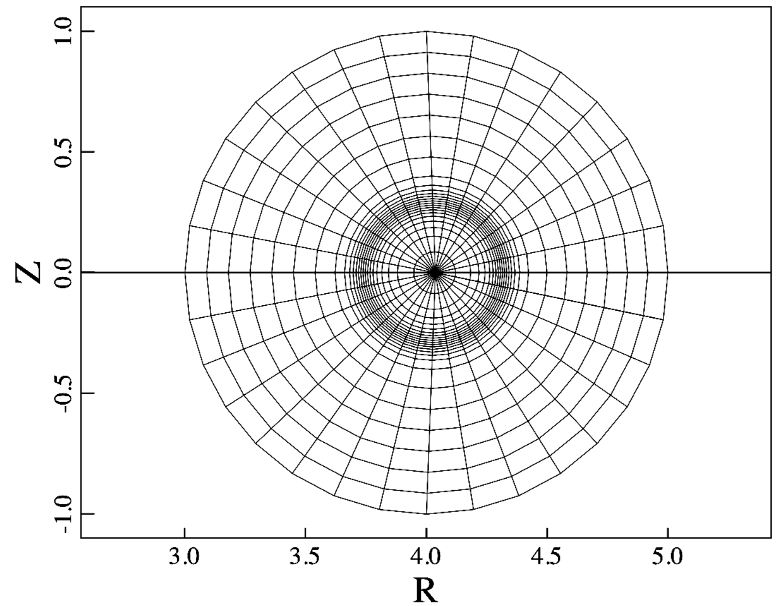

Mesh of spectral elements reflects slight Shafranov shift and is packed near 1/1 resonance.

Moderate and high resolution computations obtain a nonlinearly increasing kinetic energy growth-rate.

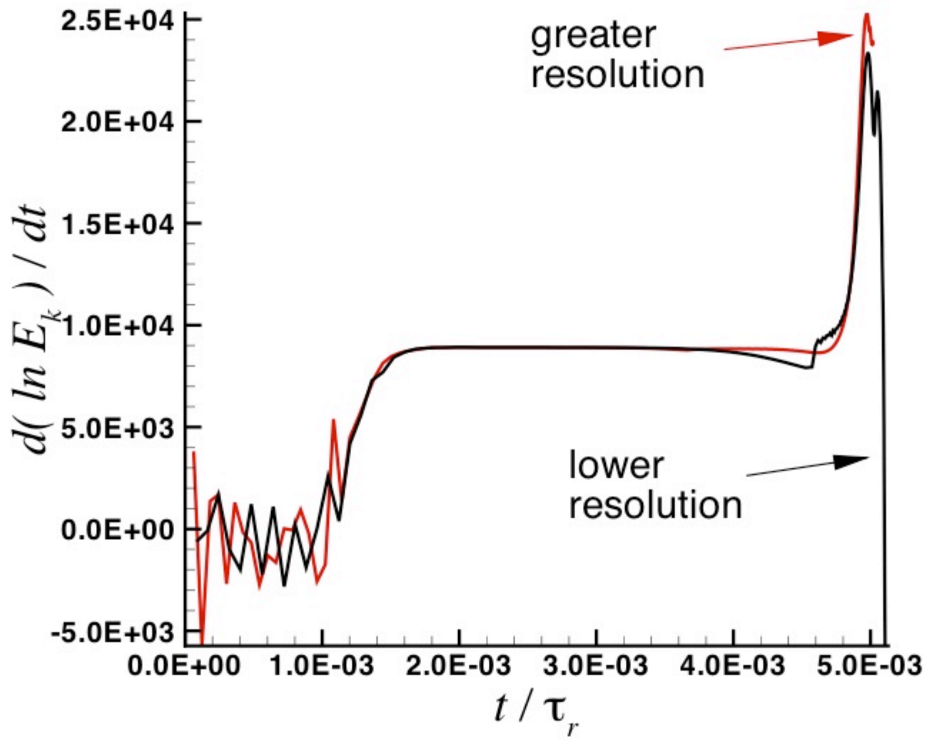

- First case has a 20×20 mesh, degree of polynomials is 8, and $0 \leq n \leq 42$.
- Second case has a 24×32 mesh, degree of polynomials is 8, and $0 \leq n \leq 85$.
- The moderate and large computations were run on 300 and 1376 cores of "Franklin" in quad-core configuration.

The computations show a transition from current-sheet to x-point reconnection when the growth-rate of kinetic energy increases.

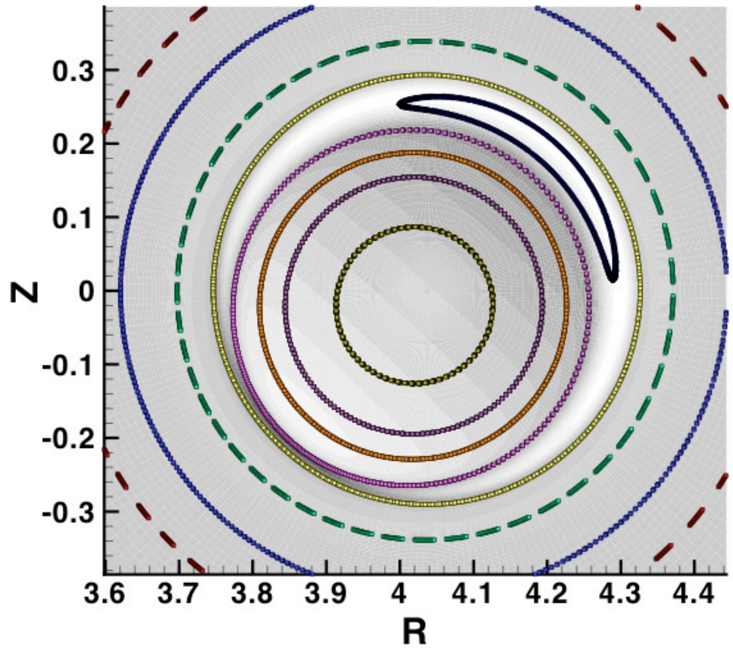

Just before the increase in growth rate (t t=4.67×10^{-3} τ_r), there is a broad layer of parallel current density (grayscale) where field-lines are reconnecting.

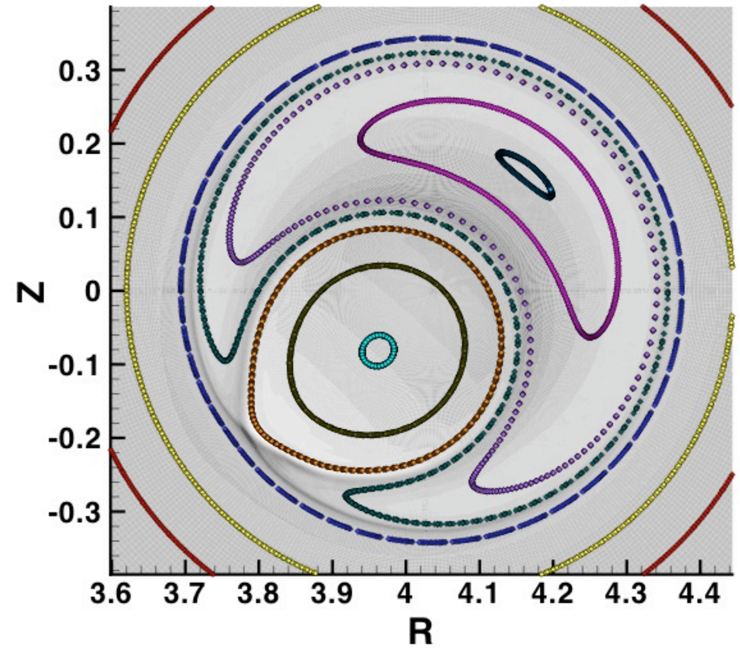

Near the peak growth rate (t t=4.95×10^{-3} τ_r), x-point reconnection is evident, and parallel current is concentrated.

- While the toroidal cases are inherently 3D, initial R/a=4 results are qualitatively similar to helically symmetric cylindrical results.

Conclusions

- Improvements to NIMROD's computational linear algebra are proving essential for studying two-fluid macroscopic dynamics in 3D.
- The implicit Hall term is non-Hermitian, but its impact on diagonal dominance is minimized by NIMROD's Fourier representation.
- Implicit electron inertia is a HPD operator and limits numerical stiffness from the *R*-mode, even with realistic m_e/m_i.
- Incorporating limited Fourier coupling is proving reasonably effective and scalable in production two-fluid computations.
- The algorithmic improvements are being used successfully in a two-fluid study of internal kink.
    - Also RFP tearing--see J. King, poster NP6.00071.
- Toroidal geometry computations are inherently 3D, but initial two-fluid results are qualitatively similar to the cylindrical results.

List of NIMROD-related Presentations, APS-DPP 2008

1. BP6.00041, Howell, NIMEQ: MHD Equilibrium Solver for NIMROD
2. BP6.00042, Sovinec, Preconditioning for Three-Dimensional Two-Fluid NIMROD Applications
3. BP6.00043, Kruger, Anisotropic Heat Transport in the Presence of Resonant Magnetic Perturbations
4. BP6.00044, Sharma, Parallel heat flow and stress tensor in toroidal plasmas
5. BP6.00046, Cone, FRC Formation and Translation Simulations with Anisotropic Viscosity
6. BP6.00047, Nelson, Results from the PSI-Center Interfacing Group
7. BP6.00048, Kim, Kinetic Studies of ICC Devices using High Order PIC in Finite Elements
8. BP6.00074, Schlutt, An. and comp. inv. of the effect of finite par. heat trans. on the form. of mag. isl. in 3-D pl. eq.
9. CP6.00018, Jenkins, Modeling of RF/MHD coupling using NIMROD and GENRAY
10. CP6.00042, Ji, Relaxation of non-Maxwellian moments: an. solutions of the kinetic equation for uniform plasmas
11. CP6.00044, Cheng, Progress on the Kinetic MHD model
12. CP6.00070, Ebrahimi, Finite pressure effects in the Reversed Field Pinch
13. CP6.00075, Zhu, Nonlinear Ballooning Filament: Structure and Growth
14. CP6.00077, Squires, Dynamic Behavior of Peeling-Ballooning Modes in a Shifted-Circle Tokamak
15. GO3.00013, Granetz, Studies of runaway electrons during disruptions in Alcator C-Mod
16. GP6.00025, Murphy, Magnetic reconnection with asymmetry in the outflow direction
17. JP6.00012, Bird, Numerical Simulation of MHD Relaxation during Non-Inductive Startup of STs
18. JP6.00065, Izzo, Simulation of DIII-D Plasma Shutdown by Deuterium Dilution Cooling
19. NO3.00001, Weatherford, Spheromak Simulation in 3+1 Dimensions Using Multiscale Space/Time Spectral Elements
20. NP6.00028, Suzuki, Linear stability of resistive interchange modes in a cylindrical RFP plasma
21. NP6.00071, King, Numerical Studies of Nonlinear Two Fluid Tearing Modes in Cylindrical RFPs
22. NP6.00139, O'Bryan, Computational study of a non-ohmic flux compression startup method for STs
23. PO3.00013, Wu, 1-D Modeling of Massive Particle Injection (MPI) in Tokamaks
24. UP6.00023, Carey, MHD stability of extragalactic jets with azimuthal rotation
25. TP6.00087, McLean, Final Results from the SSPX Spheromak Program
26. TP6.00089, Stewart, Virtual diagnostics in NIMROD simulations for direct comparison to SSPX measurements
27. TP6.00090, Romero-Talamas, Numerical and experimental investigations of helicity sustainment in spheromaks
28. TP6.00092, Cohen, The Relationship of the n=1 Column Mode to Spheromak Formation
29. TP6.00091, Hooper, Spheromak aspect-ratio effects on poloidal flux amplification
30. TP6.00093, Lodestro, Multipulsed edge-current drive in a spheromak
31. TP6.00101, Akcay, NIMROD Simulations of Decaying and Driven Hit-SI Plasmas
32. TP6.00105, Macnab Extended MHD Simulations of the Formation, Merging, and Heating of Compact Tori
33. TP6.00118, Held, Numerical methods for anisotropic heat transport in high-temperature plasmas
34. UP6.00035, Forest, MHD Modeling of a Plasma Dynamo Experiment
35. YP6.00076, Takahashi, Kinetic effects of energetic particles on resistive MHD stability
36. YP6.00089, Brennan, Helical phase lag between coupled nonlinear res. MHD instabilities in toroidal flow shear